

Formation studies and controlled production of carbon nanohorns using continuous *in situ* characterization techniques

Meng-Dawn Cheng¹, Doh-Won Lee¹, Bin Zhao¹, Hui Hu¹, David J Styers-Barnett¹, Alexander A Puretzky¹, David W DePaoli¹, David B Geohegan¹, Emory A Ford² and Peter Angelini¹

¹ Oak Ridge National Laboratory, Oak Ridge, TN 37831, USA

² Materials Technology Institute, St Louis, MO 63141, USA

Received 11 December 2006, in final form 13 March 2007

Published 11 April 2007

Online at stacks.iop.org/Nano/18/185604

Abstract

The formation of carbon nanohorns by laser ablation was investigated using a scanning differential mobility analyzer combined with an ultrafine condensation particle counter. The measurement technique provided time-resolved size distributions for the carbon nanoparticles every minute during the course of the production run. The instrument performance was reasonably stable most of the time; however, during laser ablation, shockwave oscillations leading to significant transient flow and pressure variations were shown to disrupt the DMAs ability to measure accurate distributions. On the basis of the general trend observed in the data taken during the laser-ablation experiments, we found that the geometric mean diameter of the produced population shifted to larger particle sizes with increases in pulse width. For a given laser peak power and repetition rate, carbon nanoparticles of mobility diameter close to 100 nm were produced in a large abundance using longer laser pulse lengths (e.g., 10 ms) as compared to the shorter pulse lengths (e.g., 1 ms). A quantitative assessment of the particle size dispersion (using statistics like the geometric standard deviation) in relation to the laser pulse width could not be done with certainty as the shockwave disturbances produced by the laser-ablation process caused significant disruption to SMPS measurements. When laser ablation was not in operation, it was found that carbon nanoparticles with mobility diameters centred at about 20 nm could be produced by thermally desorbing the previously deposited carbon nanoparticles from the reactor wall at temperatures greater than 1300 K.

1. Introduction

Engineered carbon-based nanomaterials have received significant attention in the past few years, but the ability to continuously monitor and control the production of engineered nanostructures is lacking. Without this ability, production may suffer from unacceptable product quality and low yields that cannot meet current demands. These materials offer enormous potential as well as challenges in scientific and technological devel-

opment, with prospects for a wide range of applications including drug delivery (Ajima *et al* 2005), energy (Geohegan *et al* 2006) and environmental (e.g., CH₄ absorption) (Iijima *et al* 2004) applications. One attraction of nanomaterials is based on their unique properties (e.g., magnetic, optical, mechanical, electronic, and biological) as compared to bulk samples that continuously or abruptly change by simply varying the size of the material on the nanoscale (1–100 nm).

The ability to produce and utilize carbon-based industrial nanomaterials is not new. For example, carbon black has been used in tyres for many years. In addition, soot particles produced by diesel and turbine engines and other forms of fossil energy consumption are a major modern environmental pollutant. However, the ability to produce precision carbon-based structures such as C₆₀, C₇₀, and single-wall carbon nanotubes or nanohorns has emerged only within the past couple of decades, although the pace to explore their uses has been extremely rapid recently.

To evolve from a laboratory bench-scale experiment of nanomaterial discovery into commercial-scale production, large-volume nanomanufacturing capabilities must be developed. Means to monitor and control the manufacturing process must be developed for precision nanomanufacturing to be realized. There are limited reports in the literature on the characterization of carbon-based nanomaterials during their formation in the context of precision nanomanufacturing. Kim and Zachariah (2006, 2005) investigated the gas-phase growth mechanisms of carbon nanotubes (CNTs) using a differential mobility analyser (DMA) and an ultrafine condensation particle counter (UCPC). They observed a CNT growth rate two orders of magnitude higher in the aerosol phase than that measured on substrates and proposed an augmented diffusion growth hypothesis for this enhancement. In addition, they classified the size of carbon nanotubes indicating that one can obtain an ‘on-the-fly’ determination of the CNT length distribution.

In this paper, we present direct DMA measurements of the production of a carbon-based nanostructure—single walled carbon nanohorns (SWNHs)—by laser ablation, and continuous in-line *in situ* characterization of SWNH population dynamics. SWNHs belong to the single wall carbon nanotube family. The nanohorns produced in this investigation have been studied via thermal gravimetric analysis, scanning electron microscopy (SEM), transmission electron microscopy (TEM), and Raman spectroscopy as shown in figure 1. The SWNHs in the figure were synthesized using 20 ms-wide laser ablation pulses. Detailed characterization of SWNHs synthesized under different laser ablation conditions will be shown in another paper.

A low-magnification SEM image (figure 1(a)) shows that SWNH aggregates have an irregular spherical morphology in a variety of diameters (in this distribution, ranging from 40 to 120 nm). A high-resolution TEM image (figure 1(b)) shows an individual SWNH aggregate, which is composed of radially oriented SWNHs with conical tips. TGA data (figure 1(c)) of SWNHs were recorded by a TA Q-500 TGA instrument with a heating rate of 5 K min⁻¹ in air. The derivative peak appearing at 893 K corresponds to the contribution from SWNHs (Zhang *et al* 2005). The Raman spectrum of SWNHs (figure 1(d)) measured by a Renishaw–Raman spectroscopy instrument ($\lambda_{\text{exc}} = 633$ nm) shows two broad peaks centred at 1317 and 1588 cm⁻¹, which can be assigned to the D-band attributed to disordered sp² carbon in defect sites of nanohorns, and the G-band associated with the tangential C–C bond stretching vibration in graphitic carbon, respectively (Bekyarova *et al* 2003, Yang *et al* 2005).

Carbon nanohorns may be used in a wide range of potential applications including absorption, filtration,

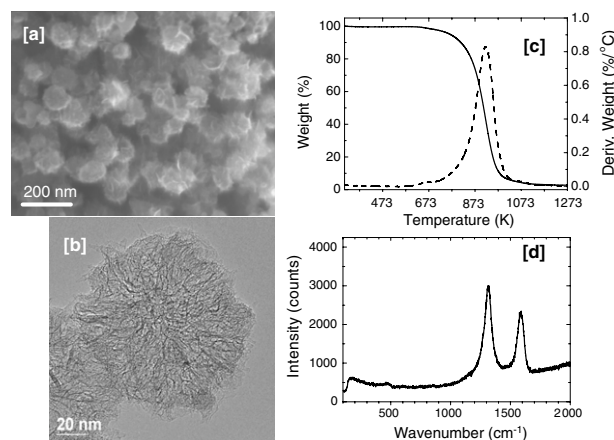


Figure 1. (a) SEM, (b) TEM, (c) TGA, and (d) Raman spectrum of SWNHs synthesized by laser ablation with 20 ms pulse width, 5 Hz repetition rate, and 94 J/pulse.

lubrication, super-capacitors, methane storage, methanol fuel cell supports, field emission, adhesives, composites, biomedical or electrical devices and much more. SWNHs can be produced in high volume and have the potential to be a low-cost material for such commercial applications. The techniques presented here demonstrate the use of continuous monitoring not only for the nanomanufacturing of carbon nanohorns, but for any nanoparticles produced by laser ablation.

2. Materials and method

SWNHs were produced in a high temperature laser ablation system as shown in figure 2. An industrial grade Nd:YAG laser (600 W maximum average power) was used to vaporize moulded graphite targets in a tube furnace similar to that used earlier by Puretzy *et al* (2000). This laser uses a custom designed raster pattern controlled through a robotic arm to optimize the ablation of the target. Laser energy was delivered through a 0.6 mm diameter fibre optic cable and focused through an anti-reflection (AR) coated window onto a target positioned in the centre of a single zone Lindberg Blue tube furnace (7.62 cm diameter quartz tube, 1423 K maximum temperature). The ends of the quartz tube are enclosed and the entire system can be evacuated using a mechanical pump to control the growth environment. Argon at atmospheric pressure (760 Torr, 4.3 lpm flow rate) was used as the background gas to carry the nanoparticles out of the furnace and into a collection chamber fitted with a HEPA filter. While maintaining the same peak power on the target in all of the experiments (within the limits of the laser), different pulse energies (9–90 J), pulse lengths (1–20 ms), and reactor temperature (298–1423 K) were used to examine the effects of the process conditions on particle production as well as their population dynamics.

Similar to our the previous work (Cheng *et al* 2006), we used a Scanning Mobility Particle Sizer (SMPS[®] model 3936L, manufactured by TSI, Minneapolis, MN) as the primary particle sizing device. The sizer system consists of three instruments: an electrical classifier (TSI Model 3080), a long-differential mobility analyser (TSI Model 3081, LDMA) and

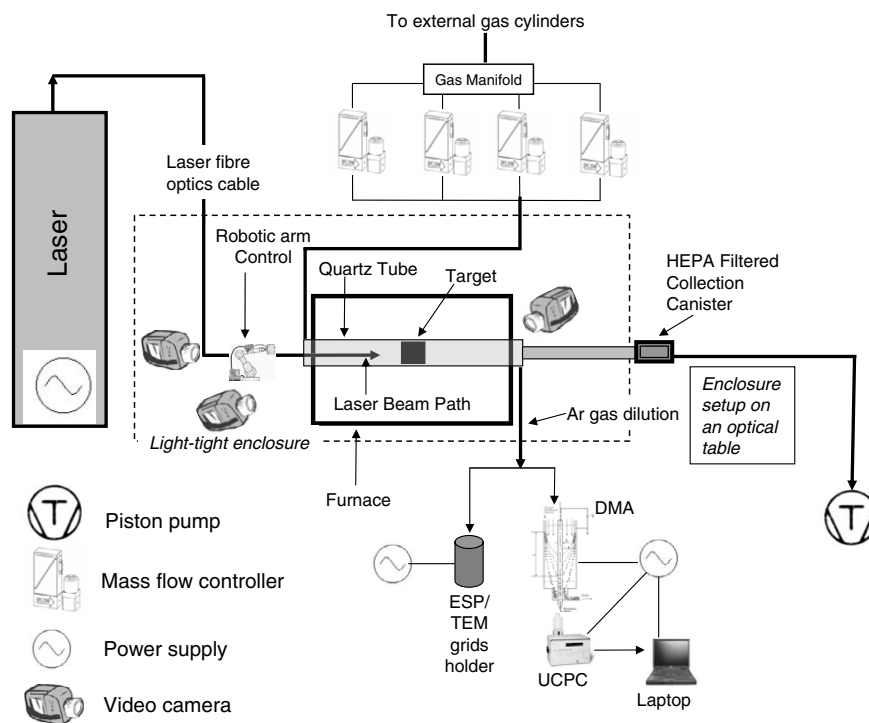


Figure 2. Experimental set-up for carbon nanoparticle production via laser ablation and instrumentation characterization.

an ultrafine condensation particle counter (TSI Model 3025A, UCPC). The ability of the SMPS to scan voltage in a defined pattern enables a DMA to be used to segregate particles based on the incrementally varied electrical voltage and thus the particle electrical mobility and size. For interested readers, Flagan (2001) and numerous references cited therein describe the principle of the electrical particle segregation technique and its use in aerosol measurement in the form of differential mobility analysis.

Particles from the laser ablation set-up (figure 2) were sampled downstream of the target through a 0.635 cm ID stainless steel line at a volumetric flow rate of 0.8 standard litres per minute (slpm) controlled by the UCPC of the SMPS. The volumetric flow rate was calibrated by using a Gilibrator[®], a primary flow standard. Ar gas was added as the dilution gas to facilitate the SMPS sampling of produced carbon nanoparticles from laser ablation in the reactor. The purpose of dilution was to freeze potential coagulation and or aggregation of the produced carbon nanoparticles by reducing the number concentration of particles in the sampling line.

Using the operating flow rate and the inlet particle impactor on the SMPS, the size range of particles measured was from about 8 to 160 nm. Each particle size distribution was measured on a 60 s interval in which there was a 50 s up scan and a 10 s down scan. Data reduction was performed on a data acquisition computer. The SMPS data were charge-corrected and the differential number concentration ($dN/d \log D_p$) and the size midpoints were exported to a spreadsheet for preliminary data analysis to generate descriptive statistics (e.g., mean, standard deviation, medium, and range).

An ORNL-designed electrostatic precipitator (ESP) was used for sampling nanoparticles to TEM grids located in a counter-sink holder on the electrode plate. The sampling

volumetric flow rate through the ESP was 0.8 slpm. This is the same precipitator used in a previous work (Mahurin and Cheng 2006). Holey carbon TEM grids (purchased from SPI Supplies, West Chester, PA, USA) were used to trap aerosol particles in the experiments for imaging using a high-resolution transmission electron microscope (HR-TEM; Hitachi HF-2000). Particle morphology and qualitative size confirmation were obtained by the HR-TEM. Although electron microscopy yields the ultimate information on aggregate morphology at the atomic scale, it is important to note that it will require imaging of a large number of particles, 10 000 for example, to obtain sufficient data for statistical inference of particle size using TEM or SEM. This would require a prohibitively large amount of time and makes it impractical to use microscopy as a tool for *in situ* process monitoring and control. In contrast, each size distribution taken by the aerosol-sizing system contains information about the size and size distribution of tens of millions of particles every minute, providing the opportunity for practical real-time process monitoring.

It is also important to note that one reads the statistics from such a particle size distribution with care when comparing to the TEM and SEM data. A SMPS-measured particle size distribution is based on the 'electrical mobility' of a particle. An electrical mobility diameter may be different from a geometric diameter that one sees under a microscope, although most of the time the two diameters are reasonably close in the range of interest to this study.

3. Results and discussion

Our experiments were designed to assess the ability of SMPS to detect changes in particle size and size distribution in the

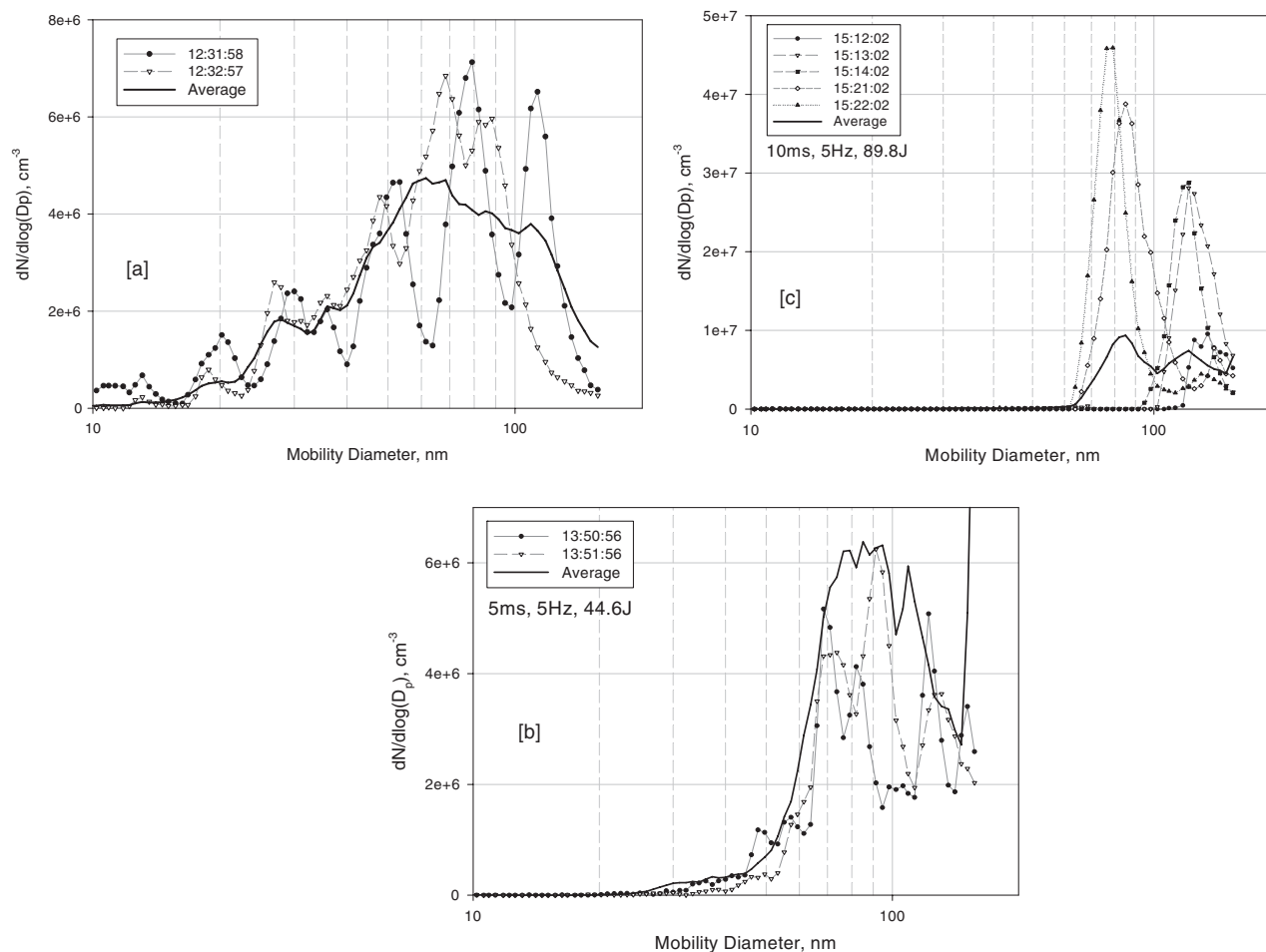


Figure 3. Plots of three individual and averaged particle size distributions for (a) case 1 (1 ms, 9.3 J/pulse); (b) case 3 (5 ms, 44.6 J/pulse); and (c) case 4 (10 ms, 90.9 J/pulse). In all the cases shown, the laser repetition rate was held constant at 5 Hz, reactor temperature at 1423 K and the laser peak power at 9 kW.

produced material—carbon nanoparticles, if any, as a result of changes in the production parameters, such as laser pulse width, repetition rate, pulse energy, and reactor temperature. Here we have focused on the effect of laser pulse width on nanohorn particle size distribution. To evaluate this, we performed a set of experiments where the repetition rate (5 Hz), reactor temperature (1423 K) and laser peak power (9 kW) were held constant and the pulse widths were changed. The laser parameters used were as follows: case 1: 1 ms, 9.3 J/pulse; case 2: 2 ms, 18.2 J/pulse; case 3: 5 ms, 45.2 J/pulse; case 4: 10 ms, 90.9 J/pulse. During the laser-ablation experiments, the SMPS measurements were significantly disturbed by the variation of flow and pressure inside the reactor caused by the expansion of shockwaves due to the pulsed laser ablation. In fact, in many instances the sampling flow to the instrument was disrupted so strongly that the instrument actually registered zero or negative flow rate for a short period of time (e.g., a few seconds). The zero-flow reading suggests the sampling flow to the instrument was temporarily choked, while the negative-flow reading indicates the reactor was temporarily vacuuming the instrument. If such a variation in flow conditions continued throughout a complete 50 s cycle, the scan could lead to a zigzag distribution curve.

This shockwave disruption was only observed during times when the laser was firing.

3.1. Measurements of particle size distributions during laser ablation

Examples of particle size distributions taken during the laser firing sessions are shown in figure 3. Figure 3(a) shows the SMPS curves from the experiments using a 1 ms pulse width, while figures 3(b) and (c) show those from 5 and 10 ms pulse widths, respectively. The average distributions for all three pulse widths are also included. The individual particle size distributions (showed with time stamps) show large oscillations instead of a smooth, Gaussian-like peak, an indication that aerosol sampling was seriously affected by the shockwaves. It is difficult to average out the shockwave oscillations with the limited number of SMPS scans available from each experiment, and it is uncertain whether such averaging is a valid approach for analysing SMPS data taken under transient conditions such as these. In short, the distributions were not suitable to make a quantitative assessment.

However, a qualitative assessment of the results shown in figure 3 suggests the 'peak' diameter of the averaged distribution for the 1 ms case was located at the 50–60 nm

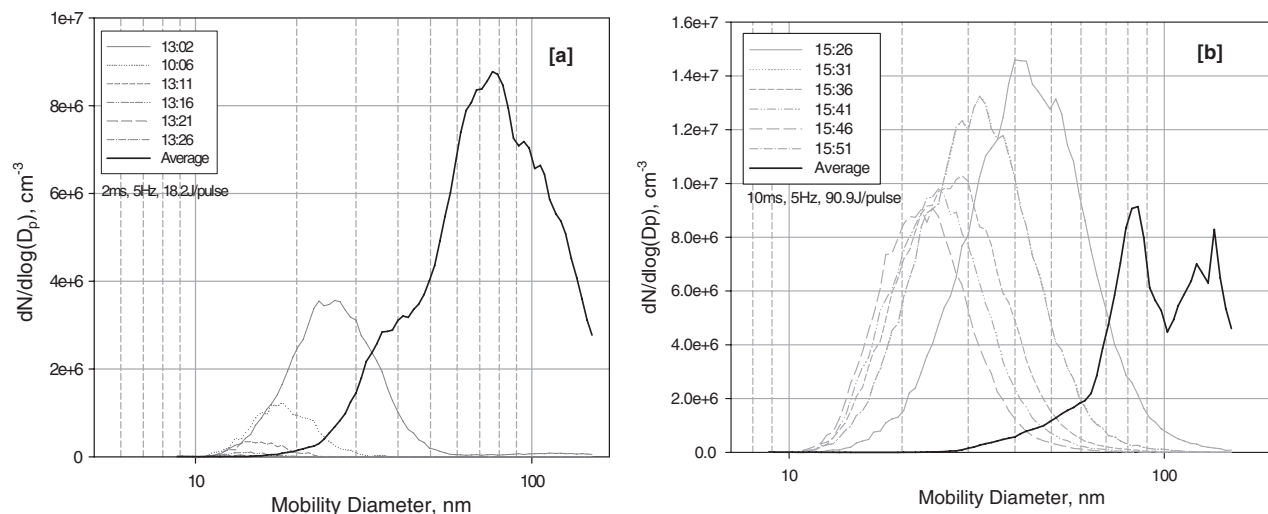


Figure 4. Plots of averaged particle size distribution during two laser-firing experiments (a) case 1 (2 ms pulse width), (b) case 4 (10 ms pulse width). Also included are the individual size distributions of particles after the laser was turned off.

region, and the average particle size increased with longer pulse widths. The average size in the 5 ms case was 80–90 nm, while there were multiple ‘peaks’ in the averaged distribution for the 10 ms case. There was one peak located at 80–90 nm, and a second peak at about 120 nm. The results show that larger aggregates of SWNHs tend to be formed using a longer laser pulse. This larger average particle size may be due to the longer pulse widths providing adequate time and particle concentration for the material to collide, forming larger and larger aggregates. In addition, at very high particle concentrations (i.e. longest pulse widths) the aggregates may be dense enough to interact, forming huge agglomerates.

3.2. Evolution of particle size distributions after laser firing ceased

In figure 4 we show two examples of the evolution of the particle size distributions. Figure 4(a) shows the example for case 2 (pulsewidth = 2 ms), and figure 4(b) shows the data for case 4 (pulsewidth = 10 ms). The averaged particle size distribution during laser firing is also included, for contrast purposes. We display the 1 min distribution every 5 min for about 25 subsequent minutes after the laser stopped firing. As a general pattern, the peak diameters of the first distribution after the laser was stopped for both cases decreased irrespective of the early history of the particle population. As the energy source (i.e., the laser) that produces the particle population was removed, the population curves shift towards smaller size. This shift in the peak diameter of the particle population was due to the outflow of the largest particles in the first minute. Since larger particles were produced only by the laser, their population would diminish as expected when the laser firing was terminated resulting in a shift towards smaller particles produced by the laser as well as from thermal desorption (see section 3.3). The further decrease in the number concentration of smaller particles was due to the balance (or unbalance) between (1) continued outflow of the laser produced particles from the reactor and (2) slower production of nanoparticles by thermal desorption of deposited carbon material on the quartz

tube wall. Note that in all cases the population peak diameter decreased to a minimum value of about 20 nm.

3.3. Thermal desorption of carbon nanoparticles

On the basis of the presented data, we questioned the source of the smallest particle population, i.e., those centred around 20 nm after the laser firing was terminated. Thermal desorption of carbon nanoparticles from the reactor wall was a possibility. In this section, we present the result of our investigation on thermal desorption of material deposited on the reactor wall following laser ablation. Figure 5 displays the time-traced results of total number concentration (figure 5(a)), geometric mean diameter (figure 5(b)), and geometric standard deviation (figure 5(c)) of case 3. The time-traced plots of reactor temperature are also displayed in these plots to show the correlation between the reactor temperature and the three population statistics.

As shown in figure 5(a), the total number concentration (TNC in number of particles per cm^3) decreased by three orders of magnitude 15 min after the laser was turned off. Note that the temperature trace remained flat within this period of time. This is a clear indication that the continuing outflow of carbon particles from the reactor outpaced the particle generation by thermal desorption. Then 14 min after the laser turned off, the temperature was gradually decreased to 1225 K, and the TNC dropped at a faster rate because the supply of particles by thermal desorption was decreased.

Twenty minutes after the laser was turned off (18:34 on the time-axis), the temperature reached 1225 K and the total number concentration had decreased to a couple of hundred per cubic centimetre, five orders of magnitude lower than the initial rate when the laser was stopped. We again increased the reactor temperature at 18:33. Three minutes later, when the reactor temperature came back to above 1300 K, a burst of particles is observed leading to a dramatic increase of the TNC at the time point 18:36. It seems that carbon particles were rapidly desorbed from the reactor wall in millions per cubic centimetre when the reactor temperature was increased above 1300 K.

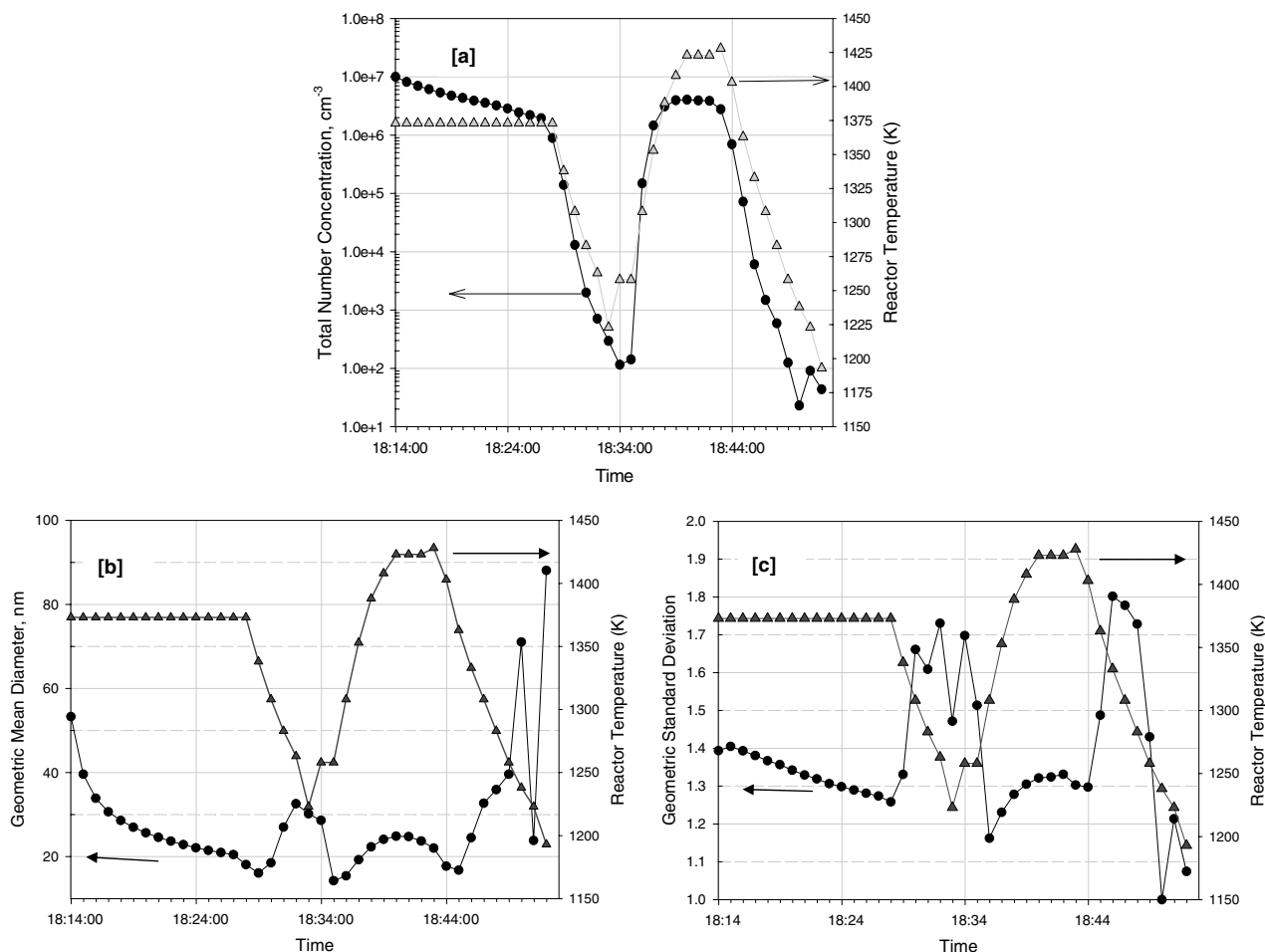


Figure 5. Plots of particle measurements made during the thermal desorption experiment after the laser was turned off at time 18:14:00. (a) total number concentration, (b) geometric mean diameter, (c) geometric standard deviation. Also plotted is the temperature time trace in the reactor during the same period of time.

During the time period from about 18:36 to 18:44, the TNC values remain reasonably steady while the reactor temperature was held above 1300 K. When the reactor temperature started to decrease at 18:43, the TNC values also started to decrease. The total number concentration of particles followed a similar decreasing trend with reactor temperature after this point to the end of the experiment. The TNC time-trace result indicates that the number concentration of particles in the reactor gas appears to positively correlate to the reactor temperature.

The GMD values in figure 5(b) of the thermally desorbed carbon nanoparticle population varied within a range from 15.5 to 24.5 nm, which is much smaller than the size of most particles produced when the laser was operating. Again, in the first 15 min when the temperature was constant, the GMD value continuously decreased from about 55 to 15 nm as the laser produced population was flushed from the furnace. Then from 18:30 to 18:34, as the temperature sharply decreased, the GMD values increased. However, note that the TNC values were in the range of 10³ during these 4 min indicating that the population statistics (GMD and GSD) should not be trusted. From 18:34 to 18:46 when temperature was increased and the TNC values increased to above 10⁶, it was found that the GMD values were also slightly increased following the

change in the reactor temperature. The correlation between the dispersion of the particle population shown in figure 5(c) and the reactor temperature follows a similar pattern as that found for the GMD. During the ‘thermal desorption’ period (between 18:35 and 18:43), the GSD value showed a small upward trend. In general, it can be seen that the GMD and GSD were independent of the reactor temperature within statistical measures.

The evidence from the population statistics shown in figure 5 suggests the possibility of particle production in the reactor through the thermal desorption mechanism. The thermally desorbed particles were quite small compared to those produced by laser ablation. The population curves of particles measured during the ‘thermal desorption’ period are shown in figure 6. The shape of these distributions suggests that the thermally desorbed particles follow a lognormal distribution. The results obtained during this test measured a peak mobility size of approximately 25 nm. This mobility size corresponds to the size of individual carbon nanohorns or the smallest carbon nanohorn aggregates, if they exist as singlets during the thermal desorption period.

We now show a plot of the log of the total number concentration of particles as a function of inverse reactor

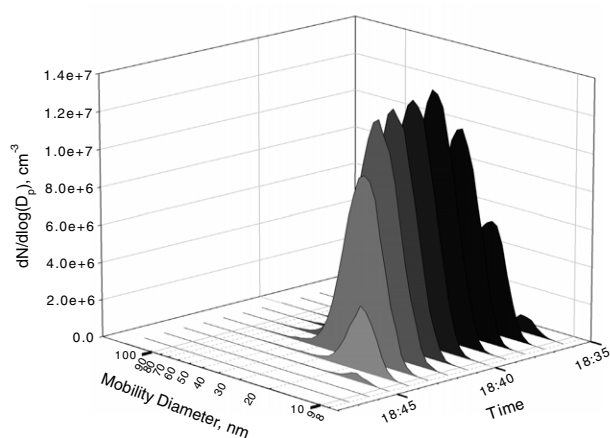


Figure 6. A three-dimensional plot of particle size distributions as a function of time during the thermal desorption experiment focusing on the time window when particles were dramatically increased, reached a stable level, and decreased when the reactor temperature was decreased. Note that dramatic change in the peak height of a distribution between the larger curves in the centre and smaller curves at both ends.

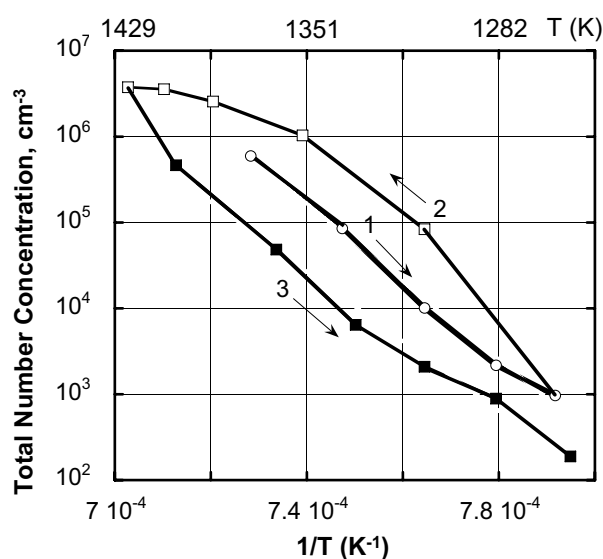


Figure 7. A plot of total number concentration of particles versus the inverse reactor temperature.

temperature in figure 7 during the thermal desorption period. As expected for an Arrhenius type equation, as the thermal energy is decreased (increase in $1/T$) the number of desorbed particles is reduced. However, total number concentration is not a measure of thermal desorption rate of particles. This could be one reason that data scatter in figure 7 was significant and that the data do not form a tight linear relationship as one would expect, if the Arrhenius equation fits.

4. Conclusions

The formation of carbon nanohorns by laser ablation was investigated using a scanning differential mobility analyzer combined with an ultrafine condensation particle counter.

The measurement technique provided time-resolved size distributions of carbon nanoparticles every minute throughout the experiments. The instrument performance was reasonably stable most of the time except during laser ablation. In other words, during laser ablation, shockwave oscillations were produced in the reactor, and these shockwaves tend to cause the instrument to produce irregular (e.g., zigzag) size distributions. In the 10 ms case the shockwaves also produced many zero particle counts. However, when using the averaged size distribution, it was found that a longer laser pulse width produced larger SWNH aggregates. When laser ablation was not in action, it was found that carbon nanoparticles with the mobility diameter centred at about 20 nm could be produced by thermally desorbing the previously deposited carbon nanoparticles from the reactor wall at temperatures greater than 1300 K. The physical and chemical nature of the thermally desorbed carbon nanoparticles is yet to be characterized, and research is ongoing to identify these small carbon nanoparticles.

Acknowledgments

Research on nanomanufacturing technology development (MDC) was funded by an MPLUS project of the Industrial Technologies Program, Office of Energy Efficiency and Renewable Energy (EERE) of the US Department of Energy (DOE), and the Materials Technology Institute (EF). Synthesis science on carbon nanostructure growth by laser vaporization (AP, DG) was funded by the Division of Materials Science and Engineering, Office of Basic Energy Sciences at DOE. Differential mobility studies (DWL) and Raman studies were performed under a user project (DSB, BZ) at the Center for Nanophase Materials Sciences, Division of Scientific User Facilities, DOE. Nanohorn characterization (HH) was funded principally by EERE Center of Excellence on Carbon-Based Hydrogen Storage, using the HF-2000 TEM at the High Temperature Materials Laboratory at ORNL. DWL, DSB, HH, and BZ were employees of the Oak Ridge National Laboratory Postdoctoral Research Associates Program administered jointly by the Oak Ridge National Laboratory and the Oak Ridge Institute for Science and Education. Oak Ridge National Laboratory is operated under the management of UT-Battelle, LLC for the US Department of Energy under Contract No. DE-AC05-00OR22725.

Disclaimers

The mention of instruments, trade names, and chemicals do not represent endorsement by the authors nor the institutions that the authors are associated with. The submitted manuscript has been authored by a contractor of the US Government under contract DE-AC05-00OR22725. © US Government.

References

- Ajima K, Yudasaka M, Murakami T, Maigné A, Shiba K and Iijima S 2005 Carbon nanohorns as anticancer drug carriers *Mol. Pharm.* **2** 475–80
- Bekyarova E *et al* 2003 Single-wall nanostructured carbon for methane storage *Phys. Chem. B* **107** 4681
- Cheng M-D, Ford E, DePaoli D W, Kenik E A and Angelini P 2006 Validation of TiO₂ particle size distribution measured by scanning mobility particle sizer *Ind. Eng. Chem.* submitted

- Flagan R C 2001 Electrical techniques *Aerosol Measurement—Principles, Techniques, and Applications* ed P Baron and K Willeke (New York, NY: Wiley-Interscience) pp 537–68
- Geohegan D B *et al* 2006 DOE FY2006 Annual Report http://www.hydrogen.energy.gov/pdfs/progress06/iv_c_1g_geohegan.pdf
- Iijima S, Murata K, Kaneko K and Yudasaka M 2004 Single walled carbon nanohorn adsorptive material and method for production thereof *US Patent Publication* 2006/0165992 A1, July 27, 2006
- Kim S H and Zachariah M R 2005 In-flight size classification of carbon nanotubes by gas phase electrophoresis *Nanotechnology* **16** 2149–52
- Kim S H and Zachariah M R 2006 In-flight kinetic measurements of the aerosol growth of carbon nanotubes by electrical mobility classification *J. Phys. Chem. B* **110** 4555–62
- Mahurin S M and Cheng M D 2006 Generating nanoscale aggregates from colloidal nanoparticles by different aerosol spray techniques *Nanotoxicology* submitted
- Puretzky A A, Geohegan D B, Fan X and Pennycook S J 2000 Dynamics of single-wall carbon nanotube synthesis by laser vaporization *Appl. Phys. A* **70** 153
- Yang C *et al* 2005 Highly ultramicroporous single-walled carbon nanohorn assemblies *Adv. Mater.* **17** 866
- Zhang M *et al* 2005 Isolating single-wall carbon nanohorns as small aggregates through a dispersion method *J. Phys. Chem. B* **109** 22201